80% Fill Factor in Organic Solar Cells with a Modified Nickel Oxide Interlayer

Garcia Romero, David; Bontekoe, Gerbrand; Pinna, Jacopo; Di Mario, Lorenzo; Ibarra-Barreno, Carolina M.; Kardula, Jane; Ersek, Gabor; Portale, Giuseppe; Rudolf, Petra; Loi, Maria Antonietta

Published in:
Advanced Energy Materials

DOI:
10.1002/aenm.202404981

Publication date:
2025

ADVANCED ENERGY MATERIALS
www.advenergymat.de

80% Fill Factor in Organic Solar Cells with a Modified Nickel Oxide Interlayer

*David Garcia Romero, Gerbrand Bontekoe, Jacopo Pinna, Lorenzo Di Mario, Carolina M. Ibarra-Barreno, Jane Kardula, Gabor Ersek, Giuseppe Portale, Petra Rudolf, and Maria Antonietta Loi**

The efficiency of organic solar cells has raised drastically in the past years. However, there is an undeniable lack of hole transport layers that can provide high carrier selectivity, low defect density, and high processing robustness, simultaneously. In this work, this issue is addressed by studying defect generation and surface passivation of nickel oxide (NiO_x). It is revealed that the generation of high oxidation state species on NiO_x surface lowers contact resistance but hinders charge extraction when employed as transport layer in organic solar cells. By using them as coordination centers, a straightforward surface modification strategy is implemented using (2-(9H-carbazol-9-yl)ethyl)phosphonic acid (2PACz) that enhances charge extraction and increases the solar cell efficiency from 11.46% to 17.12%. Additionally, the robustness of this modification across different deposition methods of the carbazole molecule is demonstrated. Finally, by fine-tuning the Fermi level using various carbazole-based molecules, and in particular with ((4-(7H-dibenzo[c,g]carbazol-7-yl)butyl)phosphonic acid (4PADCB), a power conversion efficiency of 17.29% is achieved, with an outstanding combination of a V_{OC} of 0.888 V and a fill factor of 80%.

1. Introduction

In organic solar cells, where the active layer suffers from a high exciton binding energy and low charge carrier mobilities, the power conversion efficiency, and in particular, the fill factor (FF), is heavily influenced by the charge-carrier selectivity of the device structure.[1,2] Ideal charge-carrier selective interlayers feature a combination of high transparency, high conductivity, suitable energy alignment with the active layer, and low surface trap density.[3] More importantly, the performance offered by these interlayers must be accompanied by robust processing and they have to ensure long-term device stability.

A widely used hole transport layer (HTL) which, due to its hygroscopic nature, compromises the organic solar cell stability is poly(3,4-ethylenedioxythiophene): polystyrene sulfonate (PEDOT:PSS).[4] Moreover, its low work-function induces a suboptimal energy alignment with most of the state-of-the-art p-type polymers, leading to open-circuit voltage (V_{OC}) losses.[5] Recently, ultrathin layers of p-type carbazole-based phosphonic acid molecules have been successfully employed on the bottom electrode, presenting an alternative HTL to PEDOT:PSS.[6,7] Its low thickness prevents parasitic absorption and simultaneously provides energy level tunability via chemical modification of the spacing and tail groups. Nevertheless, while they are present in the best organic solar cell efficiencies reported so far, their lack of processing robustness when employed on the bottom electrode has already been pointed out.[8] Additionally, several studies have raised concern about the possible instabilities they induce in organic solar cells.[9,10]

Metal oxide are candidates as selective interlayers for organic solar cells due to their robustness and versatile processability.[3,11] They are typically solution-processed in air from environmentally friendly nanoparticle formulations, making them ideal for potential large-scale production.[12] In particular, nickel oxide has re-emerged as a promising alternative to PEDOT:PSS and carbazole-based phosphonic acids.[13] Some early reports demonstrated that NiO_x can perform well in fullerene-based organic solar cells.[14,15] However, challenges in controlling its defect chemistry have hindered its widespread adoption in more efficient, non-fullerene-based systems.[16] As a result, NiO_x is currently not used in the best-performing organic solar cells, where the aforementioned organic counterparts are generally preferred.

The crystallization of NiO_x is typically non-stoichiometric, resulting in the formation of a large number of defects, of which the most critical ones are Ni vacancies since they determine the

D. Garcia Romero, G. Bontekoe, J. Pinna, L. Di Mario,
C. M. Ibarra-Barreno, J. Kardula, G. Ersek, G. Portale, P. Rudolf, M. A. Loi
Zernike Institute for Advanced Materials
University of Groningen
Nijenborgh 3, Groningen 9747 AG, Netherlands
E-mail: M.A.Loi@rug.nl

The ORCID identification number(s) for the author(s) of this article can be found under https://doi.org/10.1002/aenm.202404981

DOI: 10.1002/aenm.202404981

optical and electronic properties of the metal oxide. Their formation in the bulk generates a p-type doping, shifting the Fermi level and enhancing hole transport.[16–19] On the other hand, their presence on the surface has been considered detrimental to charge extraction, particularly in perovskite solar cells. Strategies to address these issues, such as passivating NiO_x surface defects with carbazole molecules, have shown promise in perovskite devices.[20,21] In the field of organic photovoltaics, the combination of NiO_x with carbazole molecules has been recently proposed as a means to mitigate active layer degradation.[10] However, the relationship between the defect chemistry of NiO_x and hole charge extraction in organic solar cells remains poorly understood. Moreover, a systematic investigation of the potential of carbazole molecules for improving NiO_x performance is still lacking.

Herein, we link the surface defects of solution-processed NiO_x to the poor behavior of the resulting organic solar cell and we propose a robust passivation strategy able to drastically improve device performance. We show that the generation of Ni^{3+} species on the surface leads to an improvement in conductivity and simultaneously provides a surface with a high concentration of coordination centers. We propose carbazole-based phosphonic acid molecules as effective surface modifiers and demonstrate chemical interaction with the Ni^{3+} species via robust surface coordination. With this new approach, the power conversion efficiency improves from 11.46% to 17.12% using (2-(9H-carbazol-9-yl)ethyl)phosphonic acid (2PACz), and also the performance of the benchmark PEDOT:PSS is surpassed, with an efficiency of 15.75%. The beneficial interaction between Ni $^{3+}$ coordination centers and the 2PACz leads to excellent processing robustness, yielding the same surface properties and solar cell performance with either spin coating or substrate immersion methods. Finally, several carbazole-based phosphonic acid small molecules with different dipole moments were employed to fine-tune the hole extraction level, and by employing (4-(7H-dibenzo[c,g]carbazol-7-yl)butyl)phosphonic acid (4PADCB) we obtain an efficiency of 17.29% and an unprecedented fill factor of 80% for nickel oxide-based organic solar cells.

2. Results and Discussion

According to previous studies, the presence of defects on NiO_x does not depend on the deposition technique (whether atomic layer deposition, sputtering, or solution-processed), and they are further generated by exposing the samples to ozone or plasma treatments.[22,18,23] These treatments have been proven to modulate the metal-oxide surface properties such as conductivity or work function.[16] When considering using NiO_x as an extraction layer for organic solar cells, we should understand how this defect affects the bulk and surface properties of the oxide, and ultimately their effect on the organic solar cell characteristics. We deposited NiO_x films in the air via spin-coating from a commercially available colloidal dispersion of nanoparticles in ethanol. The homogeneity and thickness of the thin films were optimized using atomic force microscopy (AFM) and ellipsometry (Figure S1, Supporting Information). We employ UV/Ozone as standard procedure to generate surface defects.[17,23] The drop in optical transparency observed in the UV–vis spectra of the films as UV/Ozone time is increased, implies the defect states created are located inside the bandgap (**Figure 1a**). Ellipsometry measurements showed minimal variations in the thin film thickness after treatment, confirming that the optical differences are due to a change in the material's properties.

To assess the effect of the defect generation on the organic solar cell characteristics, we fabricated cells with a structure of ITO/NiO_x/Active layer/PNDIT-3FN/Ag and tested nickel oxide films subjected to different UV/O_3 times (Figure 1b). The active layer is composed of poly[(2,6-(4,8-bis(5-(2-ethylhexyl-3-fluoro)thiophen-2-yl)-benzo[1,2-b:4,5-b']dithiophene))-alt-(5,5-(1′,3′-di-2-thienyl-5′,7′-bis(2-ethylhexyl)benzo[1′,2′-c:4′,5′-c']dithiophene-4,8-dione)] (PM6) and small molecule 2,2′-((2Z,2′Z)-((12,13-bis(2-ethylhexyl)−3,9-(2-butyloctyl)−12,13-dihydro-[1,2,5]thiadiazolo[3,4-e]thieno[2″,3″:4′,5′]thieno[2′,3′:4,5]pyrrolo[3,2-g]thieno[2′,3′:4,5]thieno[3,2-b]indole-2,10-diyl)bis-(methanylylidene))bis(5,6-difluoro-3-oxo-2,3-dihydro-1H-indene-2,1-diylidene))dimalononitrile (L8-BO). A large increase in power conversion efficiency (PCE) from 2.5% to 6% is obtained from untreated to a short UV/Ozone treatment of 2 min (Figure S2, Supporting Information). We then observe a steady improvement in efficiency, arising mainly from a steady enhancement of the V_{OC}, when the treatment time is increased up to 20 min (Figure 1c). By fitting the dark *J–V*s at high bias, we can extract the series resistance, which is directly correlated with the contact resistance of the solar cell. We observe a reduction of the series resistance from 317.4 to 101.7 Ω, indicating a decrease in the contact resistance and explaining the increased fill factor and efficiency (Figure 1d). With further increasing the treatment time, the shunt current is found to be strongly suppressed, showing that the NiO_x after the treatment can prevent shunts and effectively block electrons. However, the low built-in voltage observed across all conditions suggests a fundamental issue with the band alignment at the interface. This also indicates that the slight variation in work function that the treatment might induce does not solve the interfacial issue.

In an attempt to solve the interfacial issue, oxygen plasma and argon plasma treatments were employed on NiO_x. While these treatments improved the initial efficiency, a significant drop in the PCE was observed during the measurement indicating very poor stability (Figure S3, Supporting Information). We hypothesize that plasma, compared to ozone, produces higher Ni oxidation states which compromises the thermodynamic stability of the oxide. Therefore, we conclude that plasma treatments are too aggressive for NiO_x.[23] In parallel, the NiO_x thin film annealing temperature was optimized and found best at 140 °C, yielding the highest short-circuit current (J_{SC}) (Figure S4, Supporting Information). The lack of bandgap modulation implied that this range of temperatures does not influence the vacancy formation and the similar surface topography observed by AFM, points to a removal of ligands as the cause for such enhancement (Figures S5 and S6, Supporting Information). Similar observations have been reported for solar cells with other metal oxide nanoparticles.[24] Overall, an optimized temperature and UV/O_3 treatment leads to a champion PCE of 11.46% with a poor V_{OC} of 0.721 V and FF of 71%. These results indicate that while the formation of crystal vacancies benefits the charge transport, the hole extraction still suffers from an improper interfacial energy alignment.

Inspired by previous works on metal oxide passivation, we employ a surface modification of NiO_x using a carbazole-based

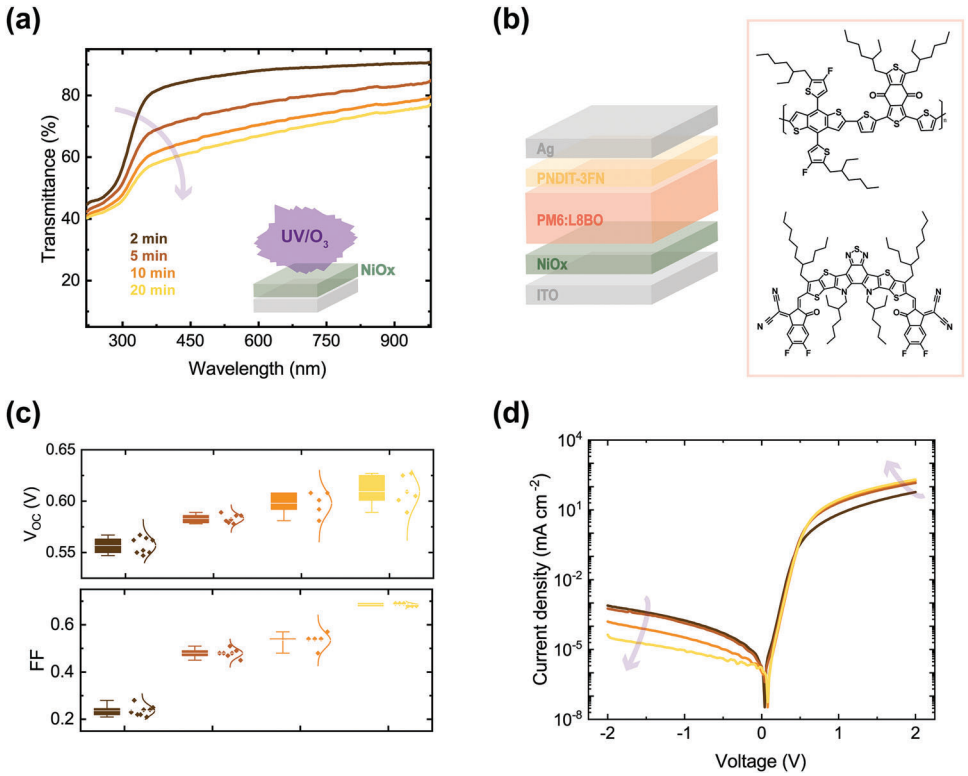

Figure 1. a) Optical transmittance of nickel oxide films subjected to different UV/Ozone treatment times (2 to 20 min). b) Solar cell structure and molecular structures of active layer components. c) Open-circuit voltage and fill factor obtained in solar cells with NiO_x as hole transport layers subjected to different UV/Ozone treatment times (2 to 20 min). d) Dark *J–V* of these solar cells.

phosphonic acid small molecule, namely (2-(9H-carbazol-9-yl)ethyl)phosphonic acid (2PACz) on the optimized UV/O_3-NiO_x films (**Figure** 2a). The change in defect density of our NiO_x films upon surface modification was evaluated by Raman spectroscopy (Figure 2b). We measured the thin films as-deposited on ITO (ref-NiO_x), after the optimized 20 min UV/O_3 treatment (UV/O_3-NiO_x) and after the surface modification (2PACz-NiO_x). The three samples show the same number of peaks: the most prominent ones being at 455 cm^{-1}, which can be ascribed to the first-order transverse optical (TO) phonon mode, and at ≈510 cm^{-1}, which corresponds to the first-order longitudinal optical (LO) phonon mode. Previous studies have shown a direct correlation between nanoparticle size and lattice distortions in NiO_x phonon excitation.[25,26] In particular, the intensity of the LO mode is correlated with the generation of metal vacancies.[25–28] As expected, the dramatic increase in the intensity of this peak after the 20 min UV/O_3 treatment points to the large creation of Ni vacancies. Interestingly, we observe a three-fold reduction in peak intensity after the 2PACz modification, suggesting that the adsorbed molecules heal the surface defects. Following a similar trend, the UV–vis absorption spectra show a sharper onset for the sample with 2PACz, indicating a reduction of intra-gap defect states and an increased transparency (Figure S7, Supporting Information). This confirms that the molecules are interacting with the optically active defects on the surface. The high energy absorption features are ascribed to the electronic transitions of the PAC molecule.

X-ray Photoelectron Spectroscopy (XPS) was employed to understand the correlation between the defect reduction and the chemical nature of the NiO_x film before (UV/O_3-NiO_x) and after 2PACz adsorption (2PACz-NiO_x) (Figure 2c). For comparison, we also measured the as-deposited NiO_x film (ref-NiO_x) (Figure S8, Supporting Information). For UV/O_3-NiO_x, the Ni2p line was deconvoluted with two components, one peaked at a binding energy (BE) of 854.2 eV and corresponding to Ni^{2+} from NiO and $Ni(OH)_2$ species and a second one peaked at a BE of 855.9 eV, ascribed to Ni^{3+} from Ni_2O_3 and NiOOH.[29,30] Taking into account our resolution, it is not reasonable to include all the complicated energy-loss peak structure of NiO_x of both oxidation states.[31] However, following the approach of previous studies evaluating Ni2*p* in NiO_x films, we have fitted our spectra using chemically reasonable species.[16,32] The O1s spectrum requires five components for a good fit; the one at the lowest BE of 529.6 eV corresponds to NiO, next, at 530.7 eV there is a component that originates from Ni_2O_3/$Ni(OH)_2$, at 531.6 eV the one ascribed to NiOOH/O—C=O and the last two components peaked at 532.6 and 533.6 eV correspond to C=O and C—OH respectively.[29,32] It is important to emphasize the ratio of intensities Ni^{3+}:Ni^{2+} increases from 2.0 (ref-NiO_x) to 2.3 (UV/O_3-NiO_x), indicating that the ozone treatment oxidizes the surface leading to the presence of more Ni^{3+} species. These results link the vacancy creation in the lattice, as concluded by Raman, to an increased Ni^{3+} population on the surface. For UV/O_3-NiO_x, O1*s* core level spectrum shows that the relative intensity of the component assigned to

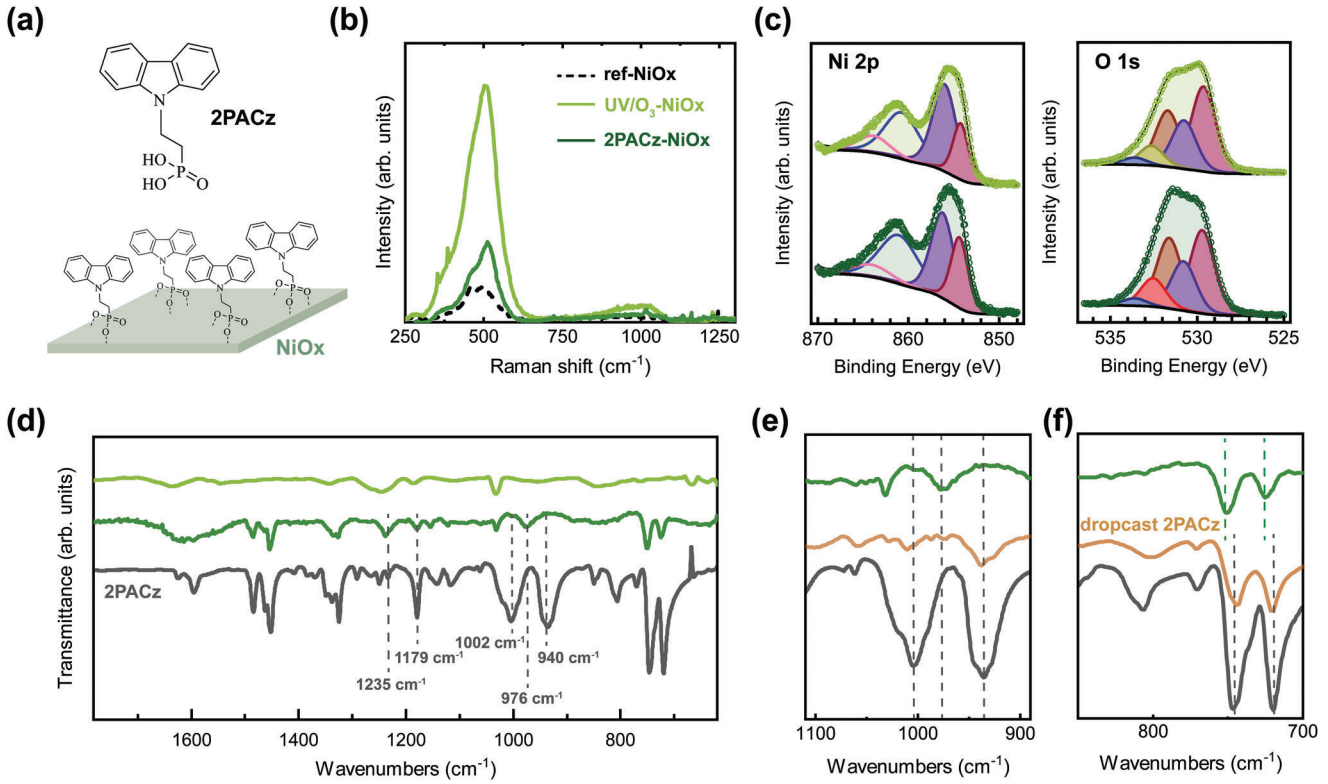

Figure 2. Surface functionalization with 2PACz molecules. a) Molecule passivation schematic. b) Raman spectra of NiO_x on ITO as deposited (NiO_x reference), after the optimized UV/Ozone treatment and NiO_x after 2PACz functionalization. c) XPS spectra of Ni 2p and O 1s core level regions of NiO_x on ITO after the optimized UV/Ozone treatment was applied (top) and following 2PACz functionalization thereafter (bottom). d-f) FTIR spectra of NiO_x after the optimized UV/Ozone treatment (light green) and after 2PACz functionalization (dark green), of 2PACz powder (black) and of 2PACz drop-casted on glass (orange).

NiOOH corresponds to 26% while that of the component attributed to $Ni_2O_3/Ni(OH)_2$ accounts only for 22.4%, confirming the presence of more OH groups at the surface after the plasma treatment, which is key for the chemisorption of 2PACz.[33] The Ni2*p* spectrum of 2PACz-NiO_x was deconvoluted with two components, one at a BE of 854.3 eV and corresponding to Ni^{2+} from NiO and $Ni(OH)_2$ and a second one at 856.2 eV BE, ascribed to Ni^{3+} from Ni_2O_3 and NiOOH.[29,33,34] The O1*s* spectrum 2PACz-NiO_x was fitted with five components; the lower BE one at 529.7 eV corresponds to NiO, the second one located at 530.7 eV is due to $Ni_2O_3/Ni(OH)_2$, the third one at 531.6 eV is ascribed to NiOOH/O—C═O and the last two components at 532.5 and 533.6 eV stem from C═O/$(PO_3)^{-1}$ and C-OH, respectively.[29,32] With respect to the O1*s* spectrum of UV/O_3-NiO_x, in the one of 2PACz-NiO_x the NiO peak decreased by 4.5% in favor of the other two components, $Ni_2O_3/Ni(OH)_2$ and NiOOH. The P2*p* core level shows a peak at 133.2 eV corresponding to the phosphonate group.[29,35] A second peak is observed at BE = 132.0 eV, which indicates that two species or two binding mechanisms occur in the phosphonate group (Figure S9a, Supporting Information). The analysis of the 2PACz-NiO_x condition leads to three conclusions. First, the increase in the atomic concentration of C and the appearance of P confirms the binding of the 2PACz on the oxide surface (Figure S9b,c, Supporting Information). Second, the Ni:O surface ratio is the same as in the UV/O_3-NiO_x, indicating that the deposited molecules are not introducing new oxygens in the lattice but reacting with the groups already present. Finally, a shift of 0.3 eV is observed for the Ni^{3+} component, indicating a chemical binding occurring between the phosphonic acid and the high oxidation state Ni species. The binding energies of the various components, their full width at half maximum (FWHM), and their relative spectral intensities are summarized in Table S1 (Supporting Information).

To gain more insights into the coordination mechanism, Attenuated Total Reflectance Fourier-Transform Infrared (ATR-FTIR) spectra were collected on NiO_x films, comparing reference NiO_x, 2PACz-NiO_x, and 2PACz powders (Figure 2d). Several bands in the spectrum of 2PACz-NiO_x were ascribed to the carbazole moiety, confirming the presence of the molecule's functional groups on the surface of NiO_x (Table S2, Supporting Information). A chemical interaction is expected to occur through phosphonic acid heterocondensation on the surface of NiO_x. Absorption bands for the symmetric and antisymmetric stretching of P—OH in the phosphonic acid moiety are observed at 940 and 1002 cm^{-1} in the 2PACz powder.[36–38] These bands are not present in the 2PACz-NiO_x sample, indicating the binding of the 2PACz goes via the hydroxy group of phosphonic acid, and the phosphonate is mainly present in the form R-$PO_3 2^-$. The broadening observed for band relative to the P═O vibration at 1179 cm^{-1} indicates that in some molecules, the double bond would participate in the surface coordination, thus leading to tridentate coordination.[39] The two distinct mechanisms expected from

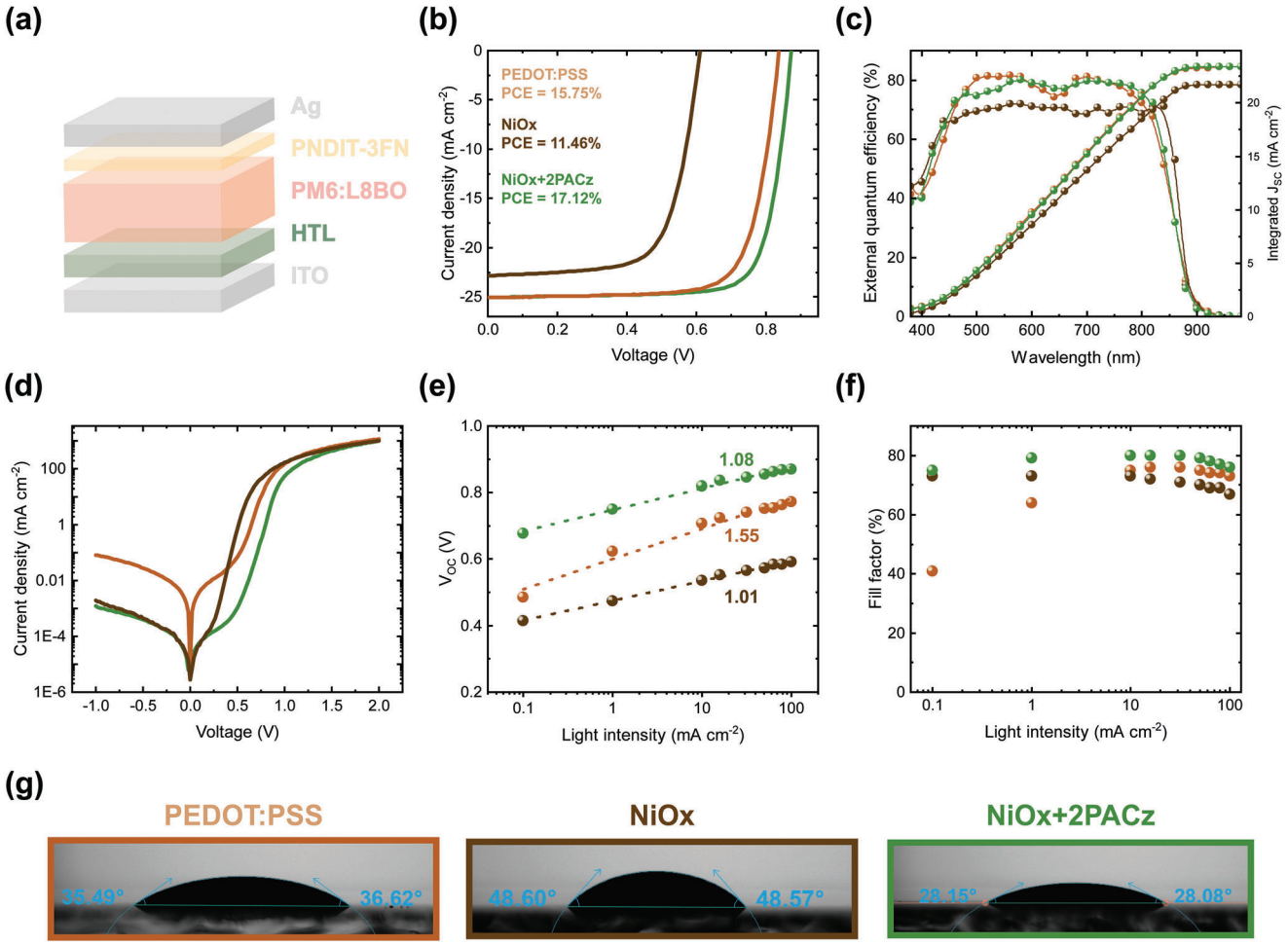

Figure 3. Photovoltaic properties comparing different hole transport layers. a) Device structure schematic. b) *J–V* characteristics employing PEDOT:PSS, NiO_x, and 2PACz-NiO_x c) External quantum efficiency and integrated short-circuit current. d) Dark *J–V* characteristics. e) Open-circuit voltage versus light intensity measurements. f) Fill factor versus light intensity measurements. g) Contact angle measurements of diiodomethane on the surface of the three transport layers: PEDOT:PSS, NiO_x, and NiO_x/2PACz.

the binding energies of the phosphorous, with the lack of a free P—O single bond stretching modes on the 2PACz-NiO_x, lead us to conclude both bidentate and tridentate mechanisms could be happening simultaneously in the hetero-condensation of 2PACz onto NiO_x. For consistency, we also performed the same measurement on drop-casted 2PACz on a glass substrate, and the same peaks corresponding to the phosphonic acid as the powder can be observed (Figure 2e). This proves that the reaction is happening when 2PACz is deposited on the NiO_x film. Finally, a blueshift of ≈6 cm^{-1} is observed for the aromatic C—H bending modes at 750–720 cm^{-1} on the 2PACz-NiO_x sample, compared to the powder and drop cast (Figure 2f). A similar shift is observed on the aromatic C=C stretching modes at 1480–1450 cm^{-1}. These shifts indicate a stabilization of the carbazole moieties, most likely through weak π–π interactions when they are bound on the NiO_x surface.

The effect of NiO_x surface functionalization on the performance of organic solar cells was then evaluated by fabricating again solar cells with the same active layer and with a structure of ITO/HTL/Active layer/PNDIT-3FN/Ag (**Figure** 3a). We compared our optimized UV/O_3-NiO_x, the modified 2PACz-NiO_x, and PEDOT:PSS. The 2PACz concentration and annealing temperature were carefully optimized (Tables S3 and S4, Supporting Information). The PCE of the NiO_x-based solar cells increases drastically from 11.46% to 17.12% with the 2PACz adsorption (Figure 3b and **Table** 1). The large enhancement is mainly determined by the high V_{OC} and FF, reaching values of 0.888 V and 78%, respectively. Moreover, this solar cell outperforms the PEDOT:PSS reference, whose champion PCE was 15.75%, with a maximum V_{OC} of 0.856 V and 75% of FF. The external quantum efficiency (EQE) measurements confirm the remarkable improvement of the solar cells with 2PACz-NiO_x as compared to those with UV/O_3-NiO_x (Figure 3c). The differences in performance can be well explained by looking at the dark characteristics and the power dependence measurements (Figure 3d,e). The low shunt current offered by both UV/O_3-NiO_x and 2PACz-NiO_x as compared to PEDOT, demonstrates more effective electron blocking and shunt prevention. No significant change in the series resistance was observed among the three conditions. The alignment problem evidenced by the dark characteristics of

Table 1. Photovoltaic parameters of organic solar cells with different hole transport layers.

HTL	J_{SC} [mA cm^{-2}]	V_{OC} [V]	FF [%]	PCE [%]
PEDOT:PSS	25.05 (24.39 ± 0.30)	0.856 (0.83 ± 0.01)	75.0 (73.90 ± 0.01)	15.75 (15.08 ± 0.29)
NiO_x	23.55 (22.78 ± 0.47)	0.721 (0.66 ± 0.05)	71.0 (69.6 ± 0.01)	11.46 (10.53 ± 0.82)
NiO_x/2PACz	24.98 (24.54 ± 0.30)	0.888 (0.875 ± 0.009)	78.0 (77.27 ± 0.01)	17.12 (16.62 ± 0.28)

our UV/O_3-NiO_x is effectively overcome by the 2PACz coordination. The inefficient interfacial charge extraction for NiO_x can be also observed from the frequency-dependent impedance measurements at close to open-circuit voltage conditions (Figure S10, Supporting Information). The low-frequency second peak in the imaginary component of the impedance observed uniquely in the UV/O_3-NiO_x condition is typical of interfacial charge accumulation due to improper charge extraction.[40] By employing the Mott-Schottky analysis, we extracted the V_{BI}, corresponding to 0.76 V for the PEDOT:PSS condition, and increased to 0.84 V for the NiO_x/2PACz. The poor energy alignment and lack of carrier selectivity in the UV/O_3-NiO_x is evidenced by the drastic drop in slope, which leads to an overestimation of the V_{BI}. This proves that the passivation favors the interface alignment. A reduction of the trap-assisted recombination can also be deduced by the reduction in the ideality factor measured for 2PACz-NiO_x, as compared to the one for PEDOT:PSS (Figure 3f). Overall, the strong capability to keep a fill factor over 75% at both low and high light intensities proves the efficient charge collection and low leakage offered by 2PACz-NiO_x. Moreover, this makes it an interesting candidate system for solar cells for low-light power conditions.

Figure 3g shows the contact angle of diiodomethane on the three HTL surfaces. The least wetting is observed on UV/O_3-NiO_x, with a contact angle of 48°, which we expect due to the high amount of hydrophilic groups on the surface. The adsorption of 2PACz reduces the contact angle to 28°, as expected when there are hydrophobic carbazole groups pointing out of the surface. The 2PACz adsorption also improves the wetting with respect to PEDOT:PSS, which shows a contact angle of 36°, and this correlates with the improved device performance. Finally, the device stability was evaluated by re-measuring the samples after four months of shelf storage in dark conditions (Figure S11, Supporting Information). The aged solar cells based on NiO_x/2PACz show an average PCE of 96.5% of the fresh value, compared to 92.5% for the UV/O_3-NiO_x and 95.5% for PEDOT:PSS. Moreover, the NiO_x/2PACz-based solar cell showed exceptional operational stability, with 85% of the initial PCE after 450 h of continuous illumination under 1 Sun conditions.

The deposition of phosphonic acid on metal-oxide contacts, such as indium tin oxide (ITO), has been described in the solar cell literature as leading to a perfect monolayer formation.[6,7] However, there are still some discrepancies concerning how the deposition methodology can influence layer homogeneity.[8] For instance, it was found by our group that substrate immersion (SI) of these molecules on ITO leads to a higher uniformity compared to the commonly used spin-coating (SC) method.[41] To check whether, in the case of NiO_x, the properties of the carbazole molecule layer depend on the deposition method we compared SC and SI methodologies (Figure S12a, Supporting Information). More details about the fabrication can be found in Experimental Methods. The surface free energy is a measure of the intermolecular forces at the interface, thus a magnitude directly correlated with the surface composition and homogeneity.[42,43] In the case of molecules adsorbed on a surface, small changes in molecular arrangement can lead to large deviations in the surface free energy (SFE).[36,43] We performed contact angle measurements with both polar and dispersive solvents, and employed the Owens, Wendt, Rabel, and Kaelble method (OWRK) to calculate the SFE of 2PACz-NiO_x grown with both methodologies. A total SFE of 49.5 and 50.8 mN m^{-1} was found for SC-2PACz-NiO_x and SI-2PACz-NiO_x, respectively, with almost identical dispersive components (Figure S12b, Supporting Information). These results indicate a similar arrangement of functional groups and comparable homogeneity. To validate this argument, we employed Kelvin-probe Force Microscopy (KPFM) to map the surface potential for the two conditions (Figure S12c, Supporting Information). We evaluated the surface potential distribution by fitting it with a Gaussian function and extracting the center, related to the Fermi level of the surface, and its standard deviation, related to the surface potential dispersion. Both SC-2PACz-NiO_x and SI-2PACz-NiO_x were evaluated, and for comparison, we also measured the surface of ITO. The difference in the surface potential center between the two methods is just ≈8 mV, indicating a significantly equal Fermi level. The extracted deviations are 9.7, 9.0, and 10.2 mV for SC-2PACz-NiO_x, SI-2PACz-NiO_x, and ITO, respectively, indicating that the potential deviation for both depositions is similar and shows even narrower distributions than a plain ITO substrate.

As a further step, we deposited the active layer (PM6:L8-BO) on top of both SC-2PACz-NiO_x and SI-2PACz-NiO_x, and analyzed the packing behavior by means of Grazing Incidence Wide-Angle X-ray Scattering (GIWAXS), as displayed in Figure S13 (Supporting Information). The crystallinity of the PM6:L8-BO blend has been intensively studied.[44–46] The pronounced diffraction peaks in the in-plane direction at $q_r \approx 0.3$ Å^{-1} and $q_r \approx 0.5$ Å^{-1} can be assigned to the (001) and (11-1) reflections from the lamellar stacking of both PM6 and L8-BO, respectively, and they give a signature on the molecular packing compactness.[46,47] The center and width of the peak were extracted by fitting using a pseudo-Voigt function and can be found in Table S5 (Supporting Information). The values obtained for both peak centers and full width at half maximum (FWHM) were found to be very similar irrespective of the preparation method used. Therefore, an equivalent coherence length associated with lamellar stacking is expected. The crystallite orientation is also very similar for the two processing methods. It can be concluded that the

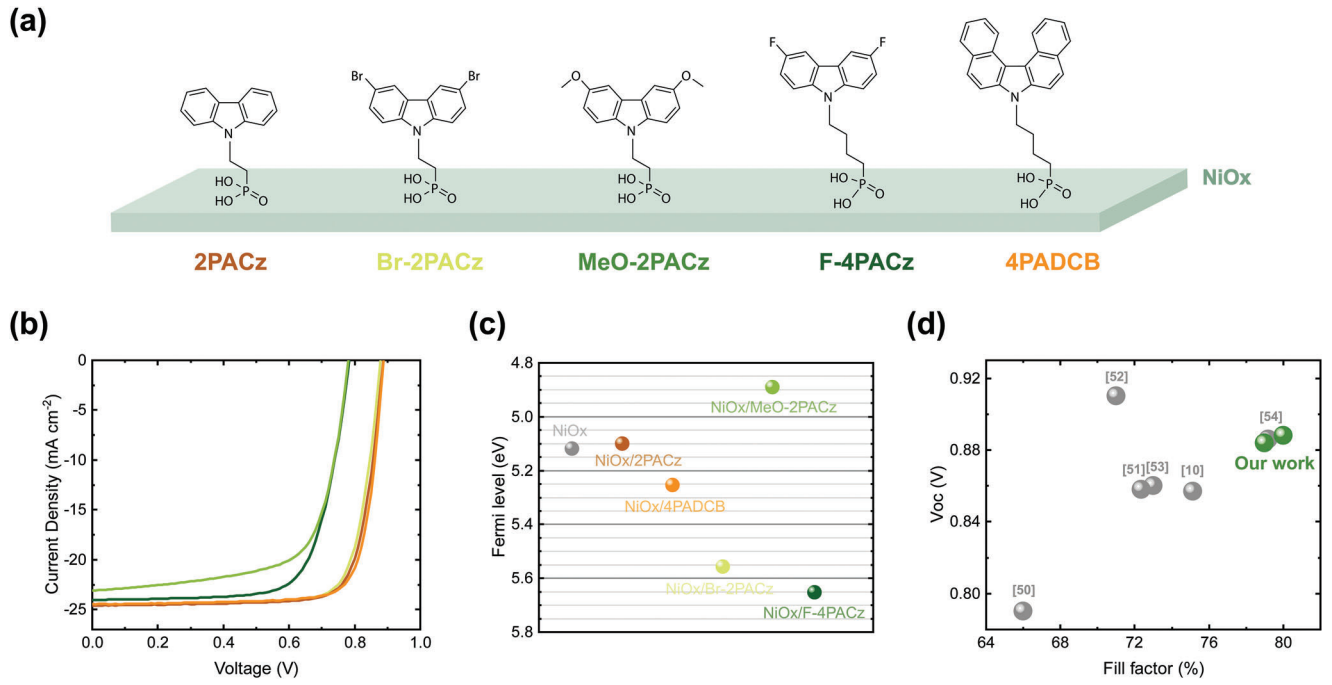

Figure 4. Surface functionalization with different carbazole-based phosphonic acid molecules. a) molecular structure of the different molecules employed on NiO_x; 2PACz, Br-2PACz, MeO-2PACz, F-4PACz, 4PADCB b) *J–V* characteristics of the solar cells – the color coding corresponds to the molecule in (a) used for modification. c) Fermi level obtained from surface potential measurements. d) Literature summary of the open-circuit voltage versus fill factor for organic solar cells using NiO_x as hole transport layer.[10,50–54]

molecular packing of the blend is not significantly influenced by the deposition method of 2PACz on NiO_x. As a last step, solar cells were fabricated with both conditions, and the *J–V* curves are displayed in Figure S14a (Supporting Information). Replicate solar cell parameters are found for SC-2PACz-NiO_x and SI-2PACz-NiO_x, and overlapped *J–V*s in dark conditions, too (Figure S14b, Supporting Information). These results confirm that the similar surface properties and crystallization of the blends on top of the NiO_x/2PACz grown by the two methods lead to the same solar cell properties. Therefore, we conclude that in contrast to previous observations on ITO substrate, the growth of 2PACz on NiO_x is very robust, leading to similar properties and solar cell performance regardless of the deposition.

Finally, to verify the universality of the NiO_x modification, we employed different carbazole-based phosphonic acid small molecules (**Figure 4**). These molecules share the anchoring group but differ in the tail and/or spacing group, generating dipoles of different strengths (Figure 4a). The Fermi level of the NiO_x after the surface modification with each of the molecules was extracted from KPFM measurements. Regardless of the molecule's tail group, the anchoring phosphonic acid has a strong affinity for the Ni^{3+} coordination centers and an on-demand Fermi level modulation can be realized. Solar cells with the modified NiO_x employing the different molecules were fabricated and compared (Figure 4b and **Table 2**). The NiO_x modified with MeO-2PACz shows the poorest performance with low V_{OC} and fill factor. The modification with F-4PACz shows an extraction barrier behavior, with a low V_{OC}. The HOMO level of PM6 has been reported to lay between 5.1 and 5.5 eV.[48,49] By looking at the Fermi level modulation, we conclude that

Table 2. Photovoltaic parameters of organic solar cells with NiO_x modified with different carbazole-based phosphonic acid molecules.

HTL	J_{SC} [mA cm^{-2}]	V_{OC} [V]	FF [%]	PCE [%]
NiO_x/2PACz	24.98	0.888	78.0	17.12
	(24.54 ± 0.30)	(0.875 ± 0.009)	(77.27 ± 0.01)	(16.62 ± 0.28)
NiO_x/Br-2PACz	24.53	0.887	78.0	16.85
	(24.29 ± 0.21)	(0.879 ± 0.003)	(76.71 ± 0.01)	(16.40 ± 0.24)
NiO_x/MeO-2PACz	23.37	0.785	68.0	12.27
	(23.03 ± 0.31)	(0.779 ± 0.003)	(67.50 ± 0.01)	(12.11 ± 0.20)
NiO_x/F-4PACz	24.05	0.797	73.0	13.84
	(23.86 ± 0.28)	(0.771 ± 0.021)	(70.7 ± 0.02)	(13.06 ± 0.76)
NiO_x/4PADCB	24.45	0.888	80.0	17.29
	(24.06 ± 0.49)	(0.886 ± 0.002)	(78.70 ± 0.02)	(16.75 ± 0.69)

NiO_x/MeO-2PACz leads to a pinning of the Fermi level far from the PM6 hole transport level, and F-4PACz leads to a hole extraction barrier (Figure 4c). In contrast to these results, modification of NiO_x using molecules with a more moderate dipole such as Br-2PACz and 4PADCB leads to a higher V_{OC} and fill factor, close to the one achieved with adsorption of 2PACz. Notably, the best device performance was realized with 4PADCB, giving a champion efficiency of 17.29% with a FF of 80% and V_{OC} of 0.888 V. To the best of our knowledge, this represents a record combination of FF and V_{OC} for organic solar cells using nickel oxide as hole transport layer (Figure 4d).

3. Conclusion

To conclude, we study the surface defect generation in NiO_x hole transport layers and propose an effective and robust molecular passivation strategy. We show that the generation of Ni^{3+} species on the metal oxide surface reduces the contact resistance and provides coordination sites for chemical bonding. We employ carbazole-based phosphonic acids as surface modifiers and describe the chemical interaction with the high oxidation state nickel species. As a result, the PCE of our solar cells increases from 11.46% to 17.12% with the modification, surpassing the performance and device stability of the standard PEDOT:PSS. The interaction between Ni^{3+} and 2PACz also makes the process adaptable to different deposition methods, maintaining consistent surface properties and solar cell performance. Finally, the use of various carbazole-based molecules with different dipole moments allows further refinement of the hole extraction level, and leads to a champion efficiency of 17.29%, with 0.888 V of V_{OC} and an 80% fill factor.

Supporting Information

Supporting Information is available from the Wiley Online Library or from the author.

Acknowledgements

This is a publication by the Focus Group "Next Generation Organic Photovoltaics" participating with the Dutch Institute for Fundamental Energy Research (DIFFER), both of which are part of the research program of the Foundation for Nederlandse Wetenschappelijk Onderzoek Instituten (NWO-I), part of the Dutch Research Council (NWO). L.D.M. and M.A.L. acknowledge funding from SOLAR-ERA.NET (project No. NFA4R2ROPV). This project was carried out with a subsidy from the Ministry of Economic Affairs and Climate Policy, Top Sector Energy subsidy scheme implemented by the Netherlands Enterprise Agency and received additional support from the Advanced Materials research program of the Zernike Institute for Advanced Materials under the Bonus Incentive Scheme (BIS) of the Netherlands Ministry of Education, Science, and Culture. The authors kindly acknowledge T. Zaharia for support with Ellipsometry measurements, and A. Kamp for technical support in the laboratory. The authors thank Prof. Wallace C.H. Choy for providing nanoparticle dispersions. The authors also acknowledge Dyenamo for providing materials for this study. GIWAXS experiments were supported by Diamond Light Source for time on Beamline I07 under proposal numbers SI36553-1.

Conflict of Interest

The authors declare no conflict of interest.

Data Availability Statement

The data that support the findings of this study are available from the corresponding author upon reasonable request.

Keywords

charge extraction, defect passivation, hole transport layer, nickel oxide, organic solar cells

Received: October 25, 2024
Revised: December 20, 2024
Published online:

[1] B. Qi, J. Wang, *Phys. Chem. Chem. Phys.* **2013**, *15*, 8972.
[2] A. Spies, M. List, T. Sarkar, U. Würfel, *Adv. Energy Mater.* **2017**, *7*, 1601750.
[3] R. Sorrentino, E. Kozma, S. Luzzati, R. Po, *Energy Environ. Sci.* **2021**, *14*, 180.
[4] J. Cameron, P. J. Skabara, *Mater. Horiz.* **2020**, *7*, 1759.
[5] M. R. Lenze, N. M. Kronenberg, F. Würthner, K. Meerholz, *Org. Electron.* **2015**, *21*, 171.
[6] Y. Lin, Y. Firdaus, F. H. Isikgor, M. I. Nugraha, E. Yengel, G. T. Harrison, R. Hallani, A. El-Labban, H. Faber, C. Ma, X. Zheng, A. Subbiah, C. T. Howells, O. M. Bakr, I. McCulloch, S. D. Wolf, L. Tsetseris, T. D. Anthopoulos, *ACS Energy Lett.* **2020**, *5*, 2935.
[7] Y. Lin, Y. Zhang, J. Zhang, M. Marcinskas, T. Malinauskas, A. Magomedov, M. I. Nugraha, D. Kaltsas, D. R. Naphade, G. T. Harrison, A. El-Labban, S. Barlow, S. De Wolf, E. Wang, I. McCulloch, L. Tsetseris, V. Getautis, S. R. Marder, T. D. Anthopoulos, *Adv. Energy Mater.* **2022**, *12*, 2202503.
[8] S. Guan, Y. Li, C. Xu, Ni Yin, C. Xu, C. Wang, M. Wang, Y. Xu, Qi Chen, D. Wang, L. Zuo, H. Chen, *Adv. Mater.* **2024**, *36*, 2400342.
[9] S. Chen, L. Feng, T. Jia, J. Jing, Z. Hu, K. Zhang, F. Huang, *Sci China Chem* **2021**, *64*, 1192.
[10] H. Xu, A. Sharma, J. Han, B. P. Kirk, A. R. Alghamdi, F. Xu, Y. Zhang, A.-H. Emwas, G. Hizalan, S. De Wolf, M. R. Andersson, G. G. Andersson, D. Baran, *Adv. Energy Mater.* **2024**, *14*, 2401262.
[11] L. Di Mario, D. Garcia Romero, H. Wang, E. K. Tekelenburg, S. Meems, T. Zaharia, G. Portale, M. A. Loi, *Adv. Mater.* **2024**, *36*, 2301404.
[12] X. Li, W. C. H. Choy, F. Xie, S. Zhang, J. Hou, *J Mater Chem A Mater* **2013**, *1*, 6614.
[13] Yi Hou, W. Chen, D. Baran, T. Stubhan, N. A. Luechinger, B. Hartmeier, M. Richter, J. Min, S. Chen, C. O. R. Quiroz, N. Li, H. Zhang, T. Heumueller, G. J. Matt, A. Osvet, K. Forberich, Z.-G. Zhang, Y. Li, B. Winter, P. Schweizer, E. Spiecker, C. J. Brabec, *Adv. Mater.* **2016**, *28*, 5112.
[14] F. Jiang, W. C. H. Choy, X. Li, D. Zhang, J. Cheng, *Adv. Mater.* **2015**, *27*, 2930.
[15] K. X Steirer, P. F. Ndione, N. E Widjonarko, M. T. Lloyd, J. Meyer, E. L. Ratcliff, A. Kahn, N. R. Armstrong, C. J. Curtis, D. S. Ginley, J. J. Berry, D. C. Olson, *Adv. Energy Mater.* **2011**, *1*, 813.
[16] E. L. Ratcliff, J. Meyer, K. X. Steirer, A. Garcia, J. J. Berry, D. S. Ginley, D. C. Olson, A. Kahn, N. R. Armstrong, *Chem. Mater.* **2011**, *23*, 4988.
[17] R. Islam, G. Chen, P. Ramesh, J. Suh, N. Fuchigami, D. Lee, K. A. Littau, K. Weiner, R. T. Collins, K. C. Saraswat, *ACS Appl. Mater. Interfaces* **2017**, *9*, 17201.
[18] C. C. Boyd, R. C Shallcross, T. Moot, R. Kerner, L. Bertoluzzi, A. Onno, S. Kavadiya, C. Chosy, E. J. Wolf, J. Werner, J. A. Raiford, C. de Paula, A. F. Palmstrom, Z. J. Yu, J. J. Berry, S. F. Bent, Z. C. Holman, J. M.

Luther, E. L. Ratcliff, N. R. Armstrong, M. D. McGehee, *Joule* **2020**, *4*, 1759.
[19] S. K. Kim, H. J. Seok, D. H. Kim, D. H. Choi, S. J. Nam, S. C. Kim, H. K. Kim, *RSC Adv.* **2020**, *10*, 43847.
[20] Z. Li, X. Sun, X. Zheng, B. Li, D. Gao, S. Zhang, X. Wu, S. Li, J. Gong, J. M. Luther, Z. A. Li, *Science.* **2023**, *382*, 284.
[21] X. Sun, C. Zhang, D. Gao, S. Zhang, B. Li, J. Gong, S. Li, S. Xiao, Z. Zhu, Z. Li, *Adv. Funct. Mater.* **2024**, *34*, 2315157.
[22] L. D'Amario, R. Jiang, U. B. Cappel, E. A. Gibson, G. Boschloo, H. Rensmo, L. Sun, L. Hammarström, H. Tian, *ACS Appl. Mater. Interfaces* **2017**, *9*, 33470.
[23] L. D'Amario, J. Föhlinger, G. Boschloo, L. Hammarström, *Chem. Sci.* **2017**, *9*, 223.
[24] D. Garcia Romero, L. Di Mario, F. Yan, C. M. Ibarra-Barreno, S. Mutalik, L. Protesescu, P. Rudolf, M. A. Loi, *Adv. Funct. Mater.* **2024**, *34*, 2307958.
[25] A. C. Gandhi, J. Pant, S. D. Pandit, S. K. Dalimbkar, T. S. Chan, C. L. Cheng, Y. R. Ma, S. Y. Wu, *J. Phys. Chem. C* **2013**, *117*, 18666.
[26] W. J. Duan, S. H. Lu, Z. L. Wu, Y. S. Wang, *J. Phys. Chem. C* **2012**, *116*, 26043.
[27] K. S. Usha, R. Sivakumar, C. Sanjeeviraja, V. Sathe, V. Ganesan, T. Y. Wang, *RSC Adv.* **2016**, *6*, 79668.
[28] M. Terlemezoglu, O. Surucu, M. Isik, N. M. Gasanly, M. Parlak, *Appl Phys A Mater Sci Process* **2022**, *128*, 50.
[29] A. R. M. Alghamdi, M. Yanagida, Y. Shirai, G. G. Andersson, K. Miyano, *ACS Omega* **2022**, *7*, 12147.
[30] Y. S. Chen, J. F. Kang, B. Chen, B. Gao, L. F. Liu, X. Y. Liu, Y. Y. Wang, L. Wu, H. Y. Yu, J. Y. Wang, Q. Chen, E. G. Wang, *JPhD* **2012**, *45*, 065303.
[31] A. P. Grosvenor, M. C. Biesinger, R. S. C. Smart, N. S. McIntyre, *Surf. Sci.* **2006**, *600*, 1771.
[32] U. K. Thakur, P. Kumar, S. Gusarov, A. E. Kobryn, S. Riddell, A. Goswami, K. M. Alam, S. Savela, P. Kar, T. Thundat, A. Meldrum, K. Shankar, *ACS Appl. Mater. Interfaces* **2020**, *12*, 11467.
[33] N. Phung, M. Verheijen, A. Todinova, K. Datta, M. Verhage, A. Al-Ashouri, H. Köbler, X. Li, A. Abate, S. Albrecht, M. Creatore, *ACS Appl. Mater. Interfaces* **2022**, *14*, 2166.
[34] S. Oswald, W. Brückner, *Surf. Interface Anal.* **2004**, *36*, 17.
[35] A. Farag, T. Feeney, I. M. Hossain, F. Schackmar, P. Fassl, K. Küster, R. Bäuerle, M. A. Ruiz-Preciado, M. Hentschel, D. B. Ritzer, A. Diercks, Y. Li, B. A. Nejand, F. Laufer, R. Singh, U. Starke, U. W. Paetzold, *Adv. Energy Mater.* **2023**, *13*, 2203982.
[36] S. A. Paniagua, P. J. Hotchkiss, S. C. Jones, S. R. Marder, A. Mudalige, F. S. Marrikar, J. E. Pemberton, N. R. Armstrong, *J. Phys. Chem. C* **2008**, *112*, 7809.
[37] A. Al-Ashouri, A. Magomedov, M. Roß, M. Jost, M. Talaikis, G. Chistiakova, T. Bertram, J. A. Márquez, E. Köhnen, E. Kasparavicius, S. Levcenco, L. Gil-Escrig, C. J. Hages, R. Schlatmann, B. Rech, T. Malinauskas, T. Unold, C. A. Kaufmann, L. Korte, G. Niaura, V. Getautis, S. Albrecht, *Energy Environ. Sci.* **2019**, *12*, 3356.
[38] M. C. Zenobi, C. V. Luengo, M. J. Avena, E. H. Rueda, *Spectrochim Acta A Mol Biomol Spectrosc* **2008**, *70*, 270.
[39] J. Sun, C. Shou, J. Sun, X. Wang, Z. Yang, Y. Chen, J. Wu, W. Yang, H. Long, Z. Ying, Xi Yang, J. Sheng, B. Yan, J. Ye, *Sol. RRL* **2021**, *5*, 2100663.
[40] T. Kirchartz, W. Gong, S. A. Hawks, T. Agostinelli, R. C. I. MacKenzie, Y. Yang, J. Nelson, *J. Phys. Chem. C* **2012**, *116*, 7672.
[41] M. Pitaro, J. S. Alonso, L. Di Mario, D. Garcia Romero, K. Tran, T. Zaharia, M. B. Johansson, E. M. J. Johansson, M. A. Loi, *J Mater Chem A Mater* **2023**, *11*, 11755.
[42] B. Jańczuk, T. Białłopiotrowicz, *J. Colloid Interface Sci.* **1989**, *127*, 189.
[43] S. A. Paniagua, A. J. Giordano, O. L. Smith, S. Barlow, H. Li, N. R. Armstrong, J. E. Pemberton, J. L. Brédas, D. Ginger, S. R. Marder, *Chem. Rev.* **2016**, *116*, 7117.
[44] Z. He, S. Li, R. Zeng, Y. Lin, Y. Zhang, Z. Hao, S. Zhang, F. Liu, Z. Tang, H. Zhong, *Adv. Mater.* **2024**, *36*, 2404824.
[45] Y. Ran, C. Liang, Z. Xu, W. Jing, X. Xu, Y. Duan, R. Li, L. Yu, Q. Peng, *Adv. Funct. Mater.* **2024**, *34*, 2311512.
[46] X. Chen, Y. Li, W. Jing, T. Zhou, X. Xu, Y. Duan, L. Yu, R. Li, Q. Peng, *Angewandte Chemie – International Edition* **2024**, *63*, e202402831.
[47] S. Shoaee, H. M. Luong, J. Song, Y. Zou, T. Q. Nguyen, D. Neher, *Adv. Mater.* **2024**, *36*, 2302005.
[48] J. Yuan, Y. Zhang, L. Zhou, G. Zhang, H.-L. Yip, T-Ki Lau, X. Lu, C. Zhu, H. Peng, P. A. Johnson, M. Leclerc, Y. Cao, J. Ulanski, Y. Li, Y. Zou, *Joule* **2019**, *3*, 1140.
[49] J. Bertrandie, J. Han, C. S. P. De Castro, E. Yengel, J. Gorenflot, T. Anthopoulos, F. Laquai, A. Sharma, D. Baran, *Adv. Mater.* **2022**, *34*, 2202575.
[50] J. Cheng, X. Ren, H. L. Zhu, J. Mao, C. Liang, J. Zhuang, V. A. L. Roy, W. C. H. Choy, *Nano Energy* **2017**, *34*, 76.
[51] H. N. Tran, H. Lee, C. B. Park, N. V. Krishna, F. T. A. Wibowo, S. Y. Jang, J. Y. Kim, S. Cho, *Adv. Mater. Interfaces* **2022**, *9*, 2201274.
[52] J. Cheng, H. Zhang, Y. Zhao, J. Mao, C. Li, S. Zhang, K. S. Wong, J. Hou, W. C. H. Choy, *Adv. Funct. Mater.* **2018**, *28*, 1706403.
[53] S. Park, D. W. Kim, S. Y. Park, *Energy Technol.* **2022**, *10*, 2201191.
[54] G. Zhang, Q. Chen, Z. Zhang, Z. Gao, C. Xiao, Y. Wei, W. Li, *Adv. Mater.* **2024**, *36*, 2310630.